Magneto-optical Kerr effect in perpendicularly magnetized $(Co_2Pt_6)_n$/Pt(111) superstructures

I. Reichl, J. Zabloudil, R. Hammerling, and A. Vernes
Center for Computational Materials Science, Vienna University of Technology, Gumpendorferstr. 1a, A-1060 Vienna, Austria

L. Szunyogh and P. Weinberger
Center for Computational Materials Science, Vienna University of Technology, Gumpendorferstr. 1a, A-1060 Vienna, Austria
(Received 18 October 2005; published 2 February 2006)

Perpendicular magnetism facilitates an increase of the storage density by a factor 2–8 as compared to longitudinal recording. Besides the improved chemical and physical stability of Co/Pt superstructures compared to RE-TM alloys, a perpendicular easy axis can be obtained by selecting a suitable Co/Pt bilayer thickness ratio. For different repetition numbers $n \leqslant 6$ *ab initio* calculated Kerr angles are presented for $(Co_2Pt_6)_n$ superstructures on Pt(111) with a 6 Pt layers thick cap in a photon energy range of 1–8 eV. The calculated maximum in the Kerr rotation angle occurs at an energy close to the experimentally observed value. Assuming an exponential decay of the gradient of θ_K with respect to n, an extrapolation of the calculated data to large n was performed in order to compare the obtained results to available experimental data.

DOI: 10.1103/PhysRevB.73.054402 PACS number(s): 75.70.−i, 78.20.−e, 78.68.+m

I. INTRODUCTION

A. Media for perpendicular magneto-optic recording

Presently magneto-optical (MO) storage media promise[1,2] to provide the highest storage densities with high data security at respectable data transfer rates. Commercially available rare earth-transition metal (RE-TM) alloys (e.g., GdTbFe), however, have several deficiencies, such as, e.g., easy oxidation of the RE metal component which necessitates the application of a protective layer that in turn complicates the structure and makes manufacturing cumbersome. Furthermore, RE-TM alloys are limited to the long wavelength region because the MO Kerr rotation decreases at higher photon energies. Consequently the resolution and therefore the areal density cannot be increased considerably by using lasers with shorter wavelengths.

However, by using metallic multilayer systems highly corrosion and oxidation resistant constituents can be chosen avoiding thus the necessity of protective layers.[3] Co/Pt superstructures are much more oxidation resistant than RE-TM alloys and pulsed laser heating does not destroy the layered structure.[4,5] Co and Fe based multilayer structures are the most promising MO media with perpendicular magnetism and good blue response, Co/Pt structures proved to be the best up-to-now.[6]

It is believed that the highest areal densities can be achieved by means of perpendicular recording. Especially, in the context of the superparamagnetic limit, perpendicular recording with a soft underlayer promises several key advantages such as, e.g., a higher coercivity (much larger than the remanent magnetization) and thicker media which allow for grains with smaller diameter and a higher signal to noise ratio (SNR). Perpendicular recording will provide an areal density two to eight times higher than when using longitudinal recording. Presently, two different perpendicular media are considered: granular (Co/Cr-type) and multilayer media (Co/Pd, Co/Pt multilayers). The advantage of the former is a good SNR, that of the latter the tunability of the coercivity field and the remanent magnetization.[7] Multilayer media, however, have wavy domain walls leading to high noise. Thus a sort of domain wall pinning technique is mandatory,[8] e.g., in Coupled Granular Continuous (CGC) media, by using for example a soft underlayer with a first deposited granular Co/Cr based medium and a multilayer Co/Pd or Co/Pt structure on top. In the present investigation we will focus on one constituent of CGC materials, namely, on Co/Pt multilayer structures.

B. Experimental investigations of Co/Pt multilayer structures

Investigations of Co/Pt superstructures show that the magneto-optical and the magnetic properties are not independent of each other: the former scale with the ratio of the thicknesses of Co to Pt, t_{Co}/t_{Pt}, the latter depend inversely on this ratio.[3] The superstructure with a Co thickness of $t_{Co}=4$ Å and a Pt thickness of $t_{Pt}=12.7$ Å shows the highest Kerr rotation with a 100 % remanence and a positive nucleation field at a wavelength of $\lambda=820$ nm. Assuming a (111) surface orientation and a perpendicular lattice spacing of 2.265 Å, the thicknesses of this superstructure in monolayers (ML) are $t_{Co}=1.8$ ML and $t_{Pt}=5.6$ ML, which in the present work is abbreviated by $Co_{1.8}Pt_{5.6}$. According to Ref. 4 a Co thickness t_{Co} of less than 4 Å (1.8 ML) and a Pt thickness t_{Pt} greater than 12 Å (5.3 ML) is needed to achieve perpendicular magnetism and a 100% remanence.

Contrary to many other ferromagnetic/nonmagnetic multilayers, in Ref. 9 it was found that despite oscillations of the coercive field, in $(Co/Pt)_n$ independent of the thickness of the Co and Pt slabs and of the number of repetitions n the Co layers are coupled ferromagnetically. Moreover, from small plateaus observed in the MO images of $(0.3\text{ nm Co}/1.2\text{ nm Pt})_{15}$ films in Ref. 10 the presence of two different magnetic phases was concluded for applied fields close to saturation. Since, however, these phases most likely occur due to dynamical effects in the magnetization reversal process, they are not included in the present inves-

tigations which as described in the next section apply only to single domains.

In Ref. 3 the Kerr spectra of Co/Pt superstructures are compared with Co/Pt (bulk) alloys corresponding to different compositions in an energy range of 0.65–5.5 eV. The very high values of the Kerr rotation angles are believed to be mainly due to the concentration of Co in Co/Pt alloys since the spectra of these alloys and of the multilayers look rather similar. The insensitivity with respect to the structure of the surface is believed to result from the fact that the wavelength of the beam is about 100–1000 times larger than the thickness of a bilayer.

II. COMPUTATIONAL DETAILS

The magneto-optical properties are investigated theoretically by using the spin-polarized relativistic screened Korringa-Kohn-Rostoker[11–13] (SKKR) method, the Kubo-Greenwood equation for finite photon frequencies[14–18] and a classical optical approach that takes into account all reflections and interferences.[19,20] The layered system studied here consists of Co/Pt superstructures with a perpendicular easy axis,[4] namely $(Co_2Pt_6)_n$, on top of a fcc Pt(111) substrate such that six Pt layers form the cap. 13 Pt layers in the case of $n \leqslant 5$ and 10 Pt layers in the case of $n=6$ serve as buffer to the bulk Pt substrate.

In the calculations we assumed an undistorted lattice corresponding to a 3D fcc lattice constant of 7.4137 a.u. (bulk Pt). The calculation of the self-consistent potentials by means of the SKKR method has been performed with 30 $\vec{k}$-points in the irreducible part of the 2D Brillouin zone and 15 energy points distributed along a suitable contour in the upper complex semiplane extending from the bottom of the valence band to the Fermi level.

In the optical conductivity calculations two adaptive techniques[17] have been used which allow to achieve a precision of 10^{-3} a.u.. while integrating in $\vec{k}$-space and in the complex energy plane. The other computational parameters, e.g., a finite temperature of $T=300$ K and a lifetime broadening of 0.048 Ry are discussed in detail in Refs. 16–18. The bottom valence band energy was taken to be −1 Ry, the upper bound at the Fermi level was $\varepsilon_u=\varepsilon_F+8k_BT$, where k_B is the Boltzmann constant and ε_F the Fermi energy is equal to that of bulk Pt, namely −0.038 Ry.

The energy dependence of the Kerr rotation and ellipticity angles as well as the dependence of the Kerr angles at a fixed energy on the repetition number n in $(Co_2Pt_6)_n$/Pt(111) superstructures was also investigated. In accordance with many experimental studies, the calculations were performed in the photon energy range of $\hbar\omega=1-8$ eV. As a special energy served the energy of an UV-laser, 3 eV ($\lambda=405$ nm).

III. RESULTS AND DISCUSSIONS

A. Dielectric tensor elements of $(Co_2Pt_6)_n$/Pt(111)

It is rewarding to investigate the contribution of each layer on the magneto-optical Kerr effect (MOKE) by analyzing the layer-resolved dielectric tensor elements $\varepsilon^p_{\mu\nu}$,[18–20]

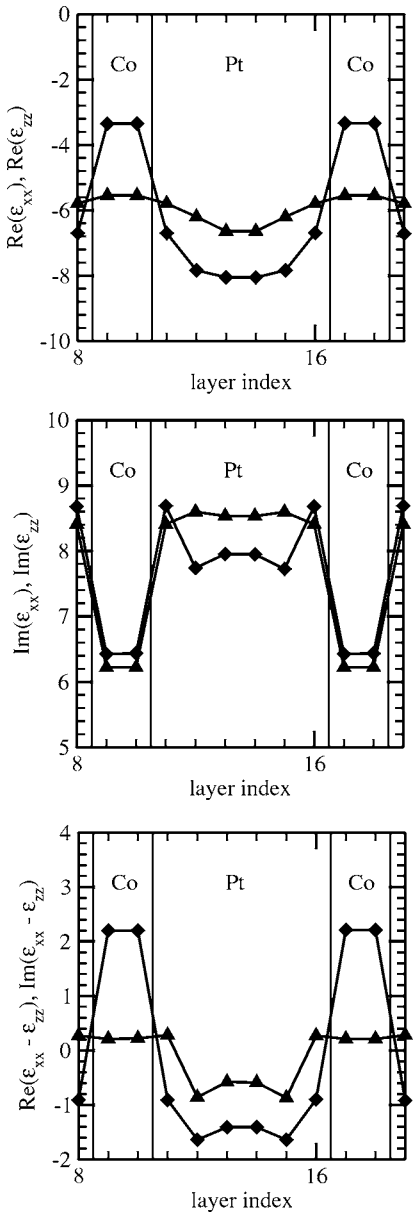

FIG. 1. Diagonal elements of the layer-resolved complex dielectric tensor, ε^p_{xx} and ε^p_{zz}, in the case of $(Co_2Pt_6)_5$/Pt(111). Note that only one unit Co_2Pt_6 is shown. The layers are labeled beginning with the last layer of the previous bilayer ($p=8$). Vertical lines denote the interfaces between Pt and Co. Diamonds refer to $\mathrm{Re}(\varepsilon^p_{xx})$ in the first, to $\mathrm{Im}(\varepsilon^p_{xx})$ in the second, and to $\mathrm{Re}(\varepsilon^p_{xx}-\varepsilon^p_{zz})$ in the third row, triangles in turn refer to $\mathrm{Re}(\varepsilon^p_{zz})$, $\mathrm{Im}(\varepsilon^p_{zz})$, and $\mathrm{Im}(\varepsilon^p_{xx}-\varepsilon^p_{zz})$.

where p numbers atomic layers and μ, ν are the Cartesian coordinates x, y, z.

Figure 1 shows the diagonal elements of the dielectric tensor, ε^p_{xx} and ε^p_{zz}. As can be seen the dielectric tensor is quite anisotropic and therefore the often used approximation $\varepsilon^p_{xx}=\varepsilon^p_{zz}$ is not appropriate in this case. The difference in the diagonal elements results from effects of spin-orbit coupling in the presence of an internal magnetic field. Note that only for a paramagnetic bulk Pt, $\varepsilon^p_{xx}=\varepsilon^p_{zz}$.

Furthermore, an analysis of $\varepsilon^p_{xx}-\varepsilon^p_{zz}$ shows that the real part of this quantity is larger in the Co layers than in the Pt

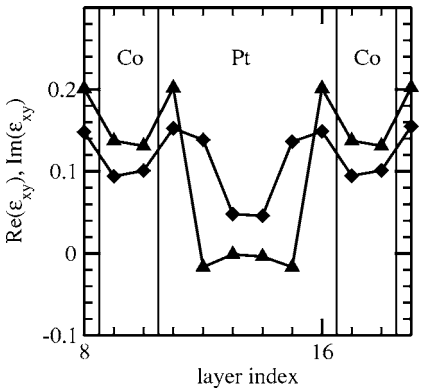

FIG. 2. Off-diagonal elements of the layer-resolved complex dielectric tensor, ε_{xy}^{p} in the case of $(Co_2Pt_6)_5/Pt(111)$. Diamonds denote $\mathrm{Re}(\varepsilon_{xy}^{p})$, triangles $\mathrm{Im}(\varepsilon_{xy}^{p})$, see also Fig. 1.

layers, whereas for the imaginary part the opposite applies. As is well known the nonvanishing off-diagonal elements of the dielectric tensor ε_{xy}^{p} lead to MO effects. In Fig. 2, it is shown that the magnitude of ε_{xy}^{p} is not largest in the Co layers but in the Pt layers adjacent to Co, Pt layers further off from the Co layers attain smaller values of $\mathrm{Re}(\varepsilon_{xy}^{p})$ and $\mathrm{Im}(\varepsilon_{xy}^{p})$. This implies that the presence of the Pt slabs is decisive for the MO Kerr effect.

For matters of completeness Fig. 3 shows the layer-resolved magnetic spin-only and the magnetic orbital-only moment as well as the sum of both. As a magnetic moment of about 0.2 μ_B is induced in the Pt layers adjacent to Co layers, this fact together with the large spin-orbit coupling of Pt explains the large contribution to the MO Kerr effect from these layers, see Fig. 2.

B. Asymptotic behavior of the polar MOKE ($n \to \infty$)

In Fig. 4 the Kerr angles at $\hbar\omega = 3$ eV are displayed for $(Co_2Pt_6)_n/Pt(111)$ with respect to the repetition number n. We will refer to the block (Co_2Pt_6) as one bilayer. Due to the finite penetration depth of the beam,[21] saturation of the Kerr rotation and ellipticity angles with respect to n is to be expected for sufficiently large n, see also Ref. 22.

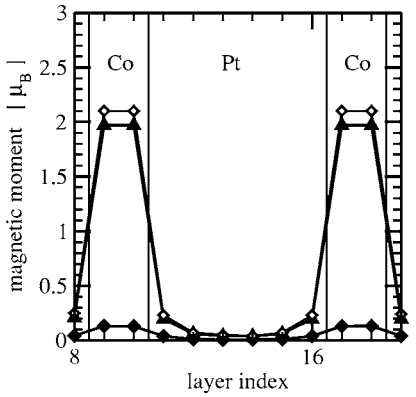

FIG. 3. Layer-resolved magnetic moments in $(Co_2Pt_6)_5/Pt(111)$. Full diamonds denote the spin-only, full triangles the orbital-only magnetic moments, the sum of both is represented by open diamonds.

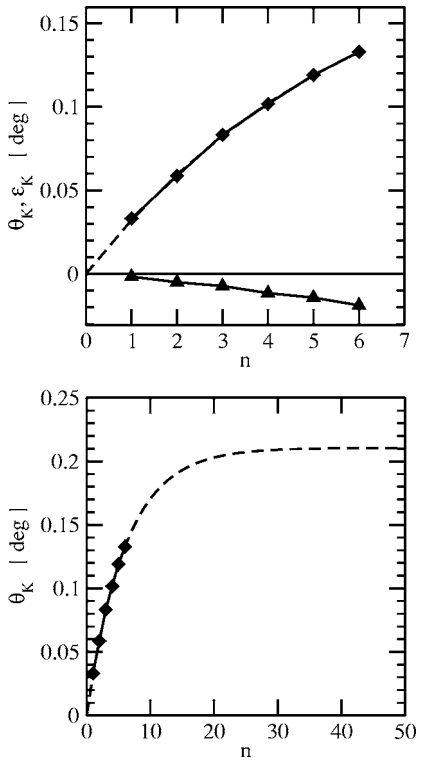

FIG. 4. MOKE for $(Co_2Pt_6)_n/Pt(111)$ superstructures at an energy of $\hbar\omega = 3$ eV. In the left part diamonds denote the Kerr rotation angle θ_K, triangles the Kerr ellipticity angle ε_K, and the dashed line an interpolation for θ_K. In the right part the extrapolation to large n is also shown.

Concerning the dependence of θ_K on the number of bilayers, the experimental findings of Ref. 4 and Ref. 22 seem to contradict each other. At 4 eV, Ref. 4 confirms Ref. 22, namely that θ_K approaches monotonically a saturation value by increasing the number of repetitions. At 1.96 eV, however, Ref. 4 shows an increase in the Kerr rotation angle until a repetition number of six, beyond this value θ_K decreases.

Since for $n=6$ the total number of atomic layers already amounts to 60, which presently is the maximum of atomic layers we can handle numerically, the problem of the saturation value can only be addressed by extrapolating the theoretical data.

For waves with a finite penetration depth an exponential damping behavior is to be expected.[21] In the following, $\theta_K(1)$ denotes the Kerr rotation angle if only one bilayer is present, $\theta_K(n)$ is that for n repetitions of Co_2Pt_6, and γ is a damping factor. Assuming that the lth bilayer (the numbering starts at the nearest bilayer to the surface, $0 \leqslant l \leqslant n-1$) contributes to $\theta_K(n)$ as the $e^{-\gamma l}$th part of $\theta_K(1)$, the Kerr rotation angle for n bilayers can be computed as follows (geometric series):

$$\theta_K(n) = \theta_K(1) \sum_{l=0}^{n-1} e^{-\gamma l} = \theta_K(1) \frac{1 - e^{-\gamma n}}{1 - e^{-\gamma}}. \qquad (1)$$

A least square fit of the theoretical data has been performed, yielding for $\hbar\omega = 3$ eV the fit parameters $\theta_K(1) = 0.0322°$ and

$\gamma=0.166$ with a quality $\chi^2=2.4\times10^{-6}$. It should be noted that according to Eq. (1) the Kerr rotation angle shows the following asymptotic behavior:

$$\lim_{n\to\infty}\theta_K(n)=\theta_K(1)\frac{1}{1-e^{-\gamma}}. \tag{2}$$

In using the above set of fitting parameters the asymptotic value of θ_K amounts to 0.2106°.

C. *Ab initio* polar MOKE at normal incidence

In Fig. 5 the experimental and calculated data for the magneto-optical Kerr rotation angle θ_K, the Kerr ellipticity angle ε_K, and the magnitude of the complex Kerr angle $\Phi_K=\sqrt{\varepsilon_K^2+\theta_K^2}$ are displayed. In Ref. 5 and in the present calculations θ_K exhibits a maximum at about 3.5 eV for $n=1,3,6$. For $n=6$ a local maximum occurs at about 1.5 eV which was also observed in Ref. 5.

The position of the maxima in the Kerr rotation angle θ_K is fairly well reproduced by the calculations. Small deviations between the peak positions in theory and experiment can be attributed to slightly different compositions, surface orientation, or surface reconstruction of the multilayer system. The absolute magnitude of the theoretical data is smaller than in experiment. As can be seen in Fig. 4, the size of the Kerr angles increases with the number of repetitions. In the experimental studies the repetition number is at least 10, whereas in the present calculation the largest value of n is 6.

Exploiting Eqs. (1) and (2), the calculated θ_K were extrapolated to $n=10$, $n=20$, and $n\to\infty$. The dependence of θ_K on the repetition number is displayed in Fig. 6 and evidently the peak at approximately 3.5 eV becomes more pronounced. In addition, in the lower part of this figure, the ratio between θ_K at $n=10$, $n=20$, and $n\to\infty$ and θ_K for the largest *ab initio* calculated system ($n=6$), is plotted versus the photon energy. For $\hbar\omega=1.36$ eV, the extrapolation was not possible since at this photon energy $d\theta_K/dn$ does not decrease. This part of Fig. 6 indicates that the scaling factor is in principle a function of the photon energy.

It should be noted that differences in geometry can lead to discrepancies between theory and experiment.[23] The present calculations are performed for normal incidence of the photon beam, the angle of incidence in the measurements, however, usually is not provided by the authors.[5,6,24] of the experimental studies. Numerous experimental as well as theoretical investigations,[25–34] however, showed that θ_K has a (material dependent) maximum at oblique incidence. If therefore the experimental investigations[5,6,24] have been performed at this very angle then our data cannot be directly compared with the measured data, as different geometries apply. The data for oblique incidence is related to the data for polar geometry by a factor which, however, is energy dependent.[35] This at least partially explains why the relative height of local maxima in θ_K (at different photon energies) is not the same in theory and experiment.

There is yet another explanation which, as described in Ref. 24, associates the size of the peaks with intermixing of Co and Pt at the interfaces. While in the low energy region

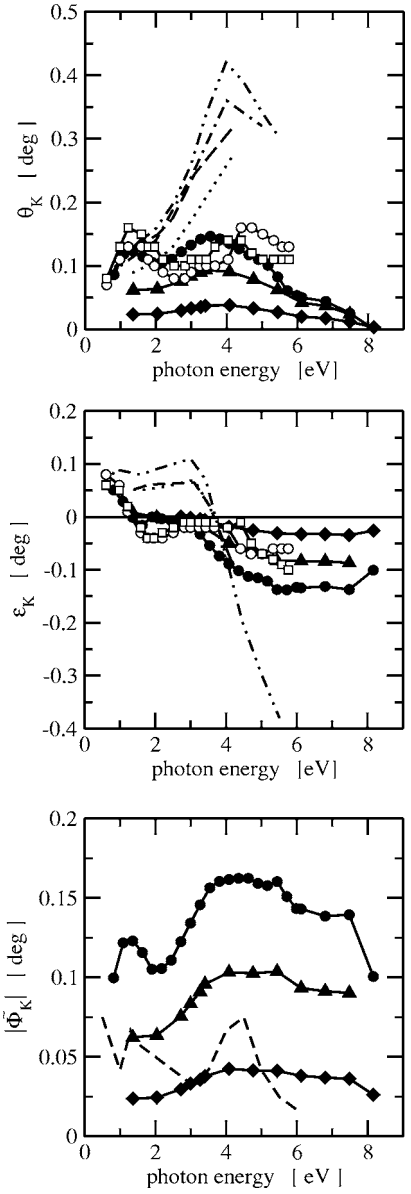

FIG. 5. Kerr rotation and ellipticity angles, θ_K and ε_K, and the magnitude of the complex Kerr angle, $|\Phi_K|$, for different photon energies. In all three entries diamonds, triangles, and circles denote the calculated Kerr quantities of $(Co_2Pt_6)_n/Pt(111)$ superstructures with repetition number $n=1$, 3, and 6, respectively. Open circles and squares refer to the calculated data for θ_K and ε_K of Ref. 24 in Co_2Pt_7 and Co_3Pt_6, respectively. Measured data for θ_K, ε_K, and Φ_K are denoted in the following way: In the case of θ_K, dashed line: $[Co(3.75\ Å)/Pt(13.5\ Å)]_{20}/Pt/Si$ (Ref. 6); dotted line: $[Co(3.75\ Å)/Pt(13.5\ Å)]_{10}/Pt/Si$ (Ref. 6); dashed-dotted line: $[Co(4.5\ Å)/Pt(17.7\ Å)]_{22}/Si$ (Ref. 5); dashed-dotted-dotted line: $[Co(3.8\ Å)/Pt(13.4\ Å)]$ on a glass substrate (Ref. 24). For ε_K, dashed line: $[Co(3.75\ Å)/Pt(13.5\ Å)]_{20}/Pt/Si$ (Ref. 6); dotted line: $[Co(3.75\ Å)/Pt(13.5\ Å)]_{10}/Pt/Si$ (Ref. 6); dashed-dotted-dotted line: $[Co(3.8\ Å)/Pt(13.4\ Å)]$ on a glass substrate (Ref. 24). Finally, Φ_K of $[Co(4.1\ Å)/Pt(19\ Å)]_{25}$ (Ref. 4) is given by a dashed line.

the height of the maxima agrees well with experiment, in the high energy region, the theory does not reproduce the measured magnitude of θ_K sufficiently well. In Ref. 24 calcula-

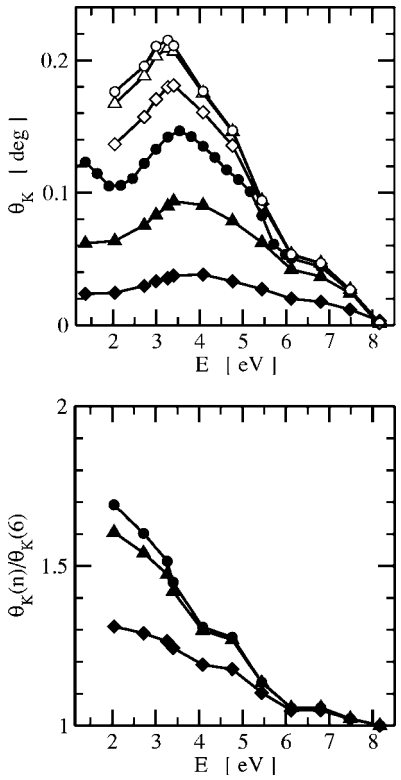

FIG. 6. Extrapolation to higher values of n. Left entry: full symbols denote the *ab initio* calculated θ_K for $n=1$ (diamonds), 3 (triangles), and 6 (circles), respectively; open symbols denote data extrapolated to $n=10$ (diamonds), 20 (triangles), and $n\rightarrow\infty$ (circles), respectively. Right entry: $\theta_K(n)/\theta_K(n=6)$ at $n=10$ (diamonds), $n=20$ (triangles), and $n\rightarrow\infty$ (circles).

tions were performed for partially alloyed interfaces in terms of a supercell approach. This kind of calculation resulted in a better agreement with the experimental data.

Different substrates can also influence the results. In Ref. 6 the Co/Pt bilayers are deposited on Pt/Si, in Ref. 11 on Si only, and in Ref. 24 a Co/Pt bilayer structure (the number of repetitions is not mentioned) is prepared on a glass substrate. Furthermore, experimental and theoretical investigations have not been performed for exactly the same Co and Pt thicknesses in one bilayer. The measurement in Ref. 6 refers to Co(3.75 Å)Pt(13.5 Å) which by assuming a (111) surface with a perpendicular, lattice spacing of 2.265 Å corresponds to a unit of $Co_{1.7}Pt_{6.0}$; the measurement in Ref. 5 on Co(4.5 Å)Pt(17.7 Å) corresponds to $Co_{2.0}Pt_{7.8}$, and in Ref. 24 Co(3.8 Å)Pt(13.4 Å) means $Co_{1.7}Pt_{5.9}$.

Finally, it should be noted that the difference between the theoretical data of Ref. 24 and our *ab initio* data are most likely caused by different computational methods applied to evaluate the optical conductivity. The authors of Ref. 24 include a phenomenological Drude term while in the present investigation the optical conductivity is calculated completely on a first-principles basis, i.e., all terms are taken into account on equal footing.

IV. CONCLUSION

In the present investigation the different contributions of Co and Pt layers to the diagonal and off-diagonal elements of the complex layer-resolved dielectric tensor were discussed. It turned out that the Pt layers are strongly polarized as was shown in terms of the layer-resolved dielectric tensor elements and the layer-resolved magnetic orbital and spin moments.

The main emphasis was put on the analysis of polar MOKE in $(Co_2Pt_6)_n$/Pt(111). Despite the fact that an *ab initio* determination of the Kerr angles is limited to systems with a smaller total number of layers than in the experiments, the peaks in the Kerr rotation angle θ_K were well reproduced. The experiments in Refs. 5, 6, and 24 show a peak at 4 eV while in our calculations the same maximum is located at 3.5 eV. In the calculations of Ref. 24 this peak is at 4 eV (Co_3Pt_6) and 4.5 eV (Co_2Pt_7), see Fig. 5. A more detailed analysis of the differences between theoretical and experimental results requires, however, the knowledge of the exact geometry applied in the measurements.

It was shown that the magneto-optical response of Co/Pt multilayer structures is favorable in an energy region beyond blue laser light (3 eV) suggesting that even higher photon energies can be used for technological purposes (e.g., to increase the storage density). As the peak in the Kerr rotation angle is rather broad, in principle, also higher energies than that of the peak center may be used and thus the size of the Co/Pt nanostructures can be further reduced, however, at the expense of a slightly smaller Kerr angle. The present calculations clearly indicate the advantages of using Co/Pt superstructures for MO storage media: higher photon energies, chemical and physical stability (Pt termination) and possibilities of reducing the size of nanostructures to be produced.

ACKNOWLEDGMENTS

Financial support from Austrian Ministries (GZ 45.531, Zl 98.366, CONEX II), the Austrian Science Foundation (W004), the Wissenschaftlich-Technisches Abkommen Austria-Hungary (A-3/03), and the Hungarian National Science Foundation (OTKA T037856, T046267) are gratefully acknowledged.

[1] R. Carey, D. M. Newman, and B. W. Thomas, J. Phys. D **28**, 2207 (1995).

[2] M. Mansuripur, *The Physical Principles of Magneto-Optic Recording* (Cambridge University Press, Cambridge 1995).

[3] W. B. Zeper, F. J. A. M. Greidanus, P. F. Garcia, and C. R. Fincher, J. Appl. Phys. **65**, 4971 (1989).

[4] E. R. Moog, J. Zak, and S. D. Bader, J. Appl. Phys. **69**(2), 880 (1991).

[5] E. R. Moog, J. Zak, and S. D. Bader, J. Appl. Phys. **69**(8), 4559 (1991).

[6] X. Gao, D. W. Thompson, and J. A. Woollam, Appl. Phys. Lett. **70**(24), 3203 (1997).
[7] R. Wood, Y. Sonobe, Z. Jin, and B. Wilson, J. Magn. Magn. Mater. **235**, 1 (2001).
[8] H. Muraoka and Y. Nakamura, J. Magn. Magn. Mater. **235**, 10 (2001).
[9] J. W. Knepper, and F. Y. Yang, Phys. Rev. B **71**, 224403 (2005).
[10] R. A. Fry, L. H. Bennett, and E. D. Torre, J. Appl. Phys. **85**, 5169 (1999).
[11] L. Szunyogh, B. Újfalussy, and P. Weinberger, Phys. Rev. B **51**, 9552 (1995).
[12] L. Szunyogh, B. Újfalussy, P. Weinberger, and J. Kollár, Phys. Rev. B **49**, 2721 (1994).
[13] B. Újfalussy, L. Szunyogh, and P. Weinberger, Phys. Rev. B **51**, 12836 (1995).
[14] D. A. Greenwood, Proc. Phys. Soc. London **71**, 585 (1958).
[15] R. Kubo, J. Phys. Soc. Jpn. **12**, 570 (1957).
[16] L. Szunyogh and P. Weinberger, J. Phys.: Condens. Matter **11**, 10451 (1999).
[17] A. Vernes, L. Szunyogh, and P. Weinberger, J. Phys.: Condens. Matter **13**, 1529 (2001).
[18] A. Vernes, L. Szunyogh, and P. Weinberger, Phase Transitions **75**, 167 (2002).
[19] A. Vernes, L. Szunyogh, and P. Weinberger, Phys. Rev. B **65**, 144448 (2002).
[20] A. Vernes, L. Szunyogh, and P. Weinberger, Phys. Rev. B **66**, 214404 (2002).
[21] I. Reichl, R. Hammerling, A. Vernes, P. Weinberger, C. Sommers, and L. Szunyogh, Phys. Rev. B **70**, 214417 (2004).
[22] G. Didrichsen, W. R. Hendern, R. Atkinson, R. J. Pollard, and I. W. Salter, J. Magn. Magn. Mater. **198**, 558 (1999).
[23] A. Vernes and P. Weinberger, Phys. Rev. B **70**, 134411 (2004).
[24] S. Uba, L. Uba, A. N. Yaresko, A. Ya. Perlov, V. N. Antonov, and R. Gontarz, J. Magn. Magn. Mater. **193**, 159 (1999).
[25] R. P. Hunt, J. Appl. Phys. **38**(4), 1652 (1967).
[26] I. Reichl, "Theoretical Investigations of Magneto-Optical Properties of Multi-Layer Systems," Ph.D. thesis, Vienna University of Technology (2005).
[27] I. Reichl, A. Vernes, P. Weinberger, L. Szunyogh, and C. Sommers, Phys. Rev. B **71**, 214416 (2005).
[28] M. N. Deeter and D. Sarid, IEEE Trans. Magn. **24**(6), 2470 (1988).
[29] M.-A. Schroeder, "Magneto-Optische Kerr-Effekte im VUV an Eisen und Eisensystemen," Ph.D. thesis, Hamburg (2000).
[30] C. Y. You and S. C. Shin, Appl. Phys. Lett. **69**(9), 1315 (1996).
[31] C. Y. You and S. C. Shin, J. Magn. Magn. Mater. **84**(1), 541 (1998).
[32] C. Y. You and S. C. Shin, J. Magn. Magn. Mater. **198–199**, 573 (1999).
[33] J. Zak, E. R. Moog, C. Liu, and S. D. Bader, J. Appl. Phys. **68**(8), 4203 (1990).
[34] Z. J. Yang and M. R. Scheinfein, J. Appl. Phys. **74**(11), 6810 (1993).
[35] A. Vernes, Philos. Mag. (in press).